Prediction of a New Layered Polymorph of FeS 2 with Fe 3+ S 2– (S 2) 1/2 2- Structure

Busheng Wang, Isabelle Braems, Shunsuke Sasaki, Frédéric Guégan, Laurent Cario, Stéphane Jobic, Gilles Frapper

Prediction of a New Layered Polymorph of FeS_2 with $Fe^{3+}S^{2-}(S_2)_{1/2}{}^{2-}$ Structure

Busheng Wang‡, Isabelle Braems†, Shunsuke Sasaki†, Frédéric Guégan‡, Laurent Cario†, Stéphane Jobic†, and Gilles Frapper*‡*

‡Applied Quantum Chemistry group, E4 team, IC2MP UMR 7285, Université de Poitiers - CNRS, 4, rue Michel Brunet TSA 51106 - 86073 Poitiers Cedex 9, France

† Université de Nantes, CNRS, Institut des Matériaux Jean Rouxel, IMN, F-44000 Nantes, France

AUTHOR INFORMATION

Corresponding Author

*E-mail : isabelle.braems@cnrs-imn.fr

*E-mail : gilles.frapper@univ-poitiers.fr

ABSTRACT

The never-elucidated crystal structure of metastable iron disulfide FeS_2 resulting from the full deintercalation of Li in Li_2FeS_2 has been cracked thanks to crystal structure prediction searches based on an evolutionary algorithm combined with first-principles calculations accounting for experimental observations. Besides the newly layered *C*2/*m* polymorph of iron disulfide, two-dimensional dynamically stable FeS_2 phases are proposed containing sulfides and/or persulfide S_2 motifs.

TOC GRAPHICS

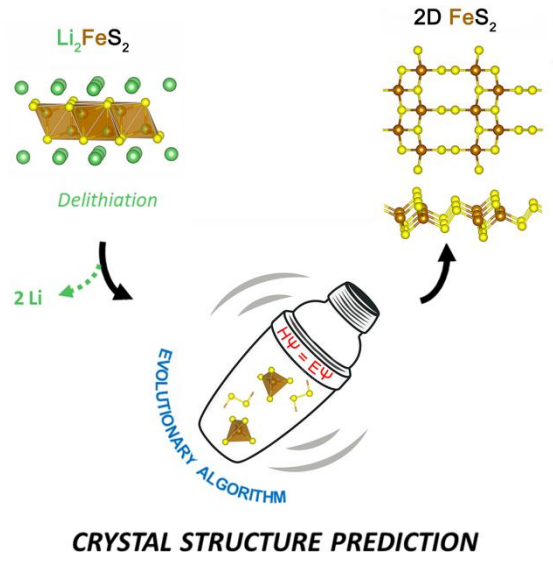

KEYWORDS

Two-dimensional material, DFT, evolutionary algorithm, iron sulfides, polymorph

Lamellar transition-metal disulfides MS_2 (M = transition element) have been intensively investigated as host lattices for chemical and electrochemical intercalation of alkali metals (*e.g.* Li, Na and K).[1–4] Indeed, these materials provided key information in the understanding of redox mechanisms in solids, and served for a while as models for secondary batteries. Simultaneously, the deintercalation process, which falls into the category of soft chemistry routes,[5,6] was used to stabilize metastable MS_2 edifices by topotactical deinsertion of the A cation from an AMS_2 pristine compound. The resulting metastable structure retains the original host features with empty A sites. For instance, metastable CdI_2-type VS_2 and cubic TiS_2 could be obtained from $LiVS_2$ and $CuTi_2S_4$ in presence of iodine and bromine as oxidizing agent, respectively.[7,8] Whatever the intercalation/deintercalation regimes, only the cationic redox center was at work in the reductive/oxidative reactions, yet one can wonder what happens to the host structure when deintercalation involves not only a cationic but also an anionic species. Such a situation was first observed for the Li_2FeS_2 ternary sulfide, which was evidenced to allow a full deintercalation of Li,[9–12] foreshadowing to some extent the forthcoming investigations on anionic redox chemistry in oxides for application in high-energy Li-ion batteries.[13–19]

Nevertheless, the metastable iron disulfide phase obtained from totally delithiated Li_2FeS_2 precursor has not been crystallographically characterized, and remains unknown. Unraveling this long-sought crystal structure is needed. Therefore, in this study we investigated thermodynamically metastable two-dimensional (2D) novel iron disfulfides FeS_2 using *ab initio* crystal structure prediction (CSP) investigations.

The Li_2FeS_2 precursor, prepared *via* a ceramic route from Li_2S and FeS, is a layered material (see Scheme 1).[20] Li_2FeS_2 may be regarded as consisting of $^2/_\infty[LiFeS_2]$ slabs with mixed Li^+/Fe^{2+} edge-sharing tetrahedral sites separated by monolayers of Li^+ cations in

octahedral coordination. The overall charge balance can be written $(Li^{+})_2(Fe^{2+})(S^{2-})_2$. While the detailed mechanism of delithiation is still under study,[21] some features have been confirmed experimentally and are ascertained: the first deintercalation of half of the Li leads to the oxidation of Fe^{2+} (d^6_{HS} configuration, HS indicates high spin) into Fe^{3+} (d^5_{HS} configuration) as evidenced by infrared (IR) and Mössbauer spectroscopies.[22–23] Beyond this composition, the complete departure of lithium results in the oxidation of the anions S^{2-} anions into S^{-} (or persulfide S_2^{2-}), as a study by IR spectroscopy of the delithiated phase[24] showed the existence of an absorption band around 469 cm^{-1} assigned unambiguously to the stretching mode of a singly-bonded $(S\text{-}S)^{2-}$ dimer. From the vibration frequency, a S-S distance of 2.12 Å could be deduced, *i.e.* a value comparable to that observed in the pyrite-type FeS_2 ($d_{S\text{-}S}$ = 2.18 Å). Complementary characterizations of this new form of iron disulfide by Mössbauer and EXAFS spectroscopies concluded to the existence of $Fe^{3+}{}_{HS}$ ion in tetrahedral sites with Fe-S distances of 2.28 Å and a $(S^{2-}:S_2^{2-})$ ratio of (2:1), so that the charge balance of this metastable FeS_2 material can be unambiguously be written as $Fe^{3+}S^{2-}(S_2)^{2-}{}_{1/2}$. Note that the existence of $Fe^{3+}{}_{HS}$ ion in tetrahedral sites is rather rare but has already been encountered in Fe-S clusters used as biological condensers within Fe-S proteins.[25] Finally, due to the crystal arrangement of the precursor (stacking of $LiFeS_2$ and Li layers), a lamellar feature is expected for FeS_2. While novel experiments comforted both the cation and anion redox chemistry encountered in layered $Li_{2-x}FeS_2$ as well as the structural features, *i.e.* tetrahedral Fe^{3+} cations and S_2^{2-} persulfides,[21] to date, the complete crystal structure of the investigated lamellar FeS_2 compound remains unknown, mainly due to a low crystallinity.

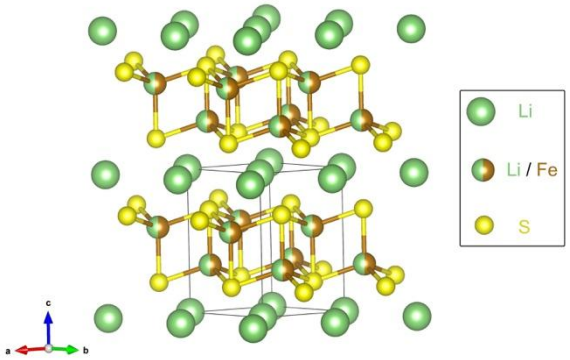

Scheme 1. Crystal structure of Li_2FeS_2. The sulfur atoms are in yellow, the lithium and iron atoms are in green and brown, respectively. Mixed Li/Fe tetrahedral sites are observed within the $LiFeS_2$ layers.

Unravelling a crystal structure of a given composition is a classical crystal structure prediction (CSP) problem that can be solved *in silico* by locating the lowest energetic phase on the potential energy surface (PES). Here, our search differs in two ways of the classical CSP problem: *(i)* the aforementioned lamellar FeS_2 compound is a metastable phase, *i.e.* its structural arrangement is expected to lie in energy significantly above the thermodynamically stable pyrite and marcasite structures,[26–30] (*ii*) the structure must meet the available experimental data, *i.e.* Fe^{3+} cations in tetrahedral coordination of sulfur atoms, and the coexistence of $(S_2)^{2-}$ dimers and sulfide anions with a 1:2 S_2^{2-}:S^{2-} ratio. Therefore, to find out the thermodynamically metastable FeS_2 phase(s), we employed a constrained fixed-composition evolutionary algorithm (EA) specifically developed in Poitiers (*constrained* EA)[31,32] that only keeps generated structures satisfying the aforementioned criteria, and discards the others. Constrained EA is based on the evolutionary algorithm method implemented in the USPEX code[33–36] that has been

successfully applied to a large number of different systems. All structure relaxations (shape, volume, and atomic positions) and energy calculations were performed with the VASP 5.4.4 code.[37] As the whole first-principles procedure involves several levels of theory to fully explore the PESs, optimize the selected low-energy FeS_2 candidates, and calculate their electronic and bonding properties, please refer to the Supporting Information for the methodology details. In the following, all structural parameters and enthalpies are given at the SCAN+U+rVV10 level of theory,[38–41] while the energy gap is computed at the hybrid Heyd-Scuseria-Ernzerhof (HSE06) functional[42] level of theory (see section S1 in the Supporting Information).

Relying on the lamellar structure of the Li_2FeS_2 host, we first investigated two-dimensional (2D) FeS_2 monolayers, then their tridimensional (3D) stacking. Using constrained EA on isolated 2D FeS_2 single layers, we located one admissible phase that crystallizes in the *C*2/*m* space group (SG n°12, *Z*=4, hereafter named *C*2/*m*-2D). Its structure type strongly differs from the MS_2 slabs commonly met in lamellar dichalcogenides where metals are six-fold coordinated by anions (octahedron or trigonal prism).[43] The *C*2/*m*-2D structure (Figure 1a) can be described as built upon one-dimensional $^1/_\infty[Fe_2S_4]$ ribbons consisting of edge-shared FeS_4 tetrahedra (mean $d_{Fe\text{-}S}$ = 2.27 Å) running along the [010] direction with zig-zag iron rows ($d_{Fe\text{-}Fe}$ = 2.82 Å). These blocks are linked to each other along the [100] axis via S-S bonds ($d_{S\text{-}S}$ = 2.03 Å) to form a corrugated $^2/_\infty[FeS_2]$ layer with characteristics in full agreement with a $(Fe^{3+})(S^{2-})(S_2^{2-})_{1/2}$ charge balance. This structure type is dynamically stable as its phonon dispersion curve does not present any imaginary frequencies in the entire Brillouin zone (see Figure 1b). We also evaluated its kinetic and thermal stabilities by running *ab initio* molecular

dynamics simulations at temperatures in the range of 300~1000 K (see the Supporting Information). All of the atoms in the 2D layer vibrate only slightly around their equilibrium positions during annealing at 300 K for 10 ps, indicating the stability of the structure at room temperature. Despite the fluctuation of atoms, the whole structure is maintained at 600 and 900 K, while the system shows reconstruction at 1000 K. This indicates that the dynamically stable structure *C*2/*m*-2D is definitively viable up to *ca*. 900 K: no structural transformations are observed in the iron and sulfur network, indicating the existence of a substantial kinetic barrier which leads to a trapping of this metastable 2D phase, in line with its experimental availability.

Finally, this layer is predicted to be a semi-conductor (HSE06 gap of 0.90 eV, see Figure S3) with antiferromagnetically coupled edge-sharing (FeS_4) tetrahedra within $1/\infty[Fe_2S_4]$ ribbons along the a axis, these ribbons been connected *via* S_2 dumbbells along the b axis (see the studied magnetic configurations in Figure S2). As indicated on the

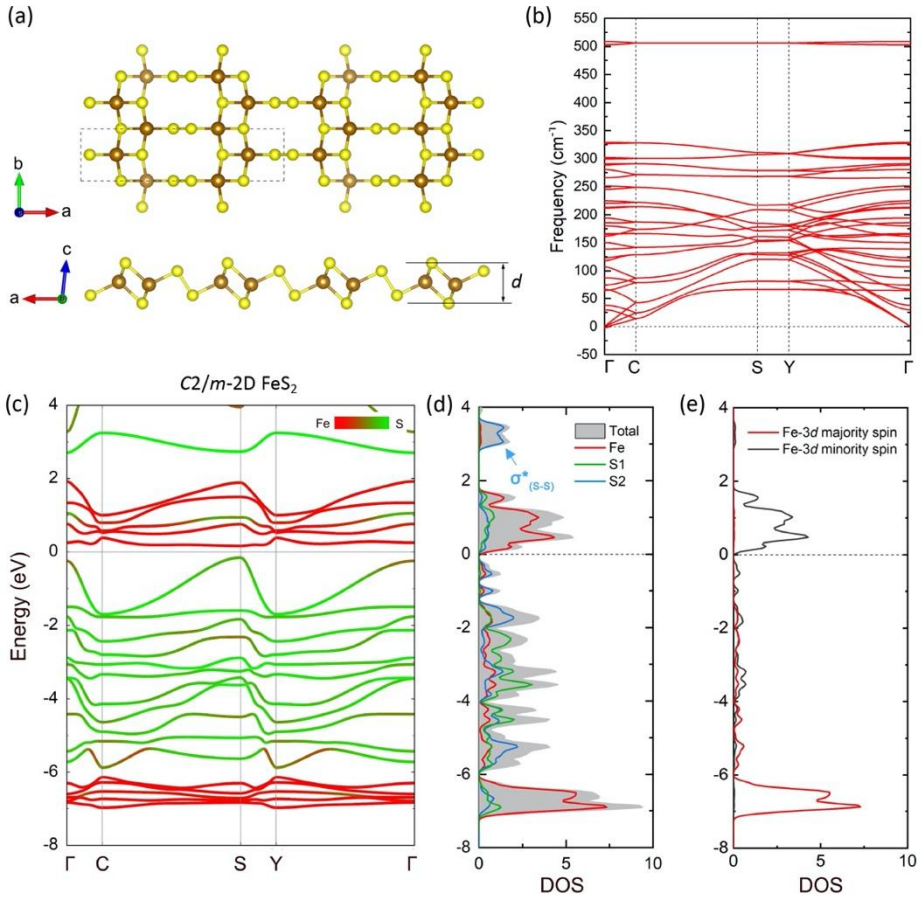

electronic density of states curve (Figure 1 d-e), the Fe 3d-spin up and spin down blocks are well separated from each other by about 6 eV while the vacant antibonding $\sigma^*_{(S-S)}$ lies much higher than these two blocks, in full agreement with the expected Fe^{3+} high spin and S_2^{2-} electronic configuration.

Figure 1. (a) Top view and side view of the FeS_2 monolayer *C*2/*m*-2D found in this work that meets all collected experimental criteria. Large brown spheres are iron atoms, yellow spheres are sulfur atoms; (b) Phonon dispersion curve with no imaginary frequency proving its dynamical stability; (c) Band structure for the *C*2/*m*-2D FeS_2, the colored bands indicate the atomic contributions to the band structure, from red (high Fe contributions) to green (high S contribution); (d) Total and projected DOS, underlying the contributions of Fe orbitals (red), sulfur atom belonging to sulfide ion S^{2-} (S_1, green), and the S-S dimer (S_2, blue); (e) Projected DOS of Fe 3d orbitals distinguishing the minority (black) and majority (red) spin contributions.

It is remarkable that this structure is more stable in energy than hypothetical 2D-FeS_2 systems deriving from 1H, 1T or distorted 1T slabs called 1T' encountered in 1H-MoS_2, 1T-MoS_2 and 1T'-MoS_2, respectively.[43,44] Both 1H-2D and 1T'-2D FeS_2 are local minima on the PES, while 1T-2D is dynamically unstable (see the Supporting Information). The enthalpy of *C*2/*m*-2D is shown to be 92 meV/f.u. lower than the 1T'-2D (with Fe in a distorted octahedron), and 633 meV/f.u. lower than the 1H-2D (with Fe in a trigonal prism) structures that are proved to be stable for other transition-metal disulfides.[43] This clearly asserts that Fe^{4+} cations are instable in sulfide environment, and that Fe^{3+} cations in tetrahedral sites are not oxidizing enough towards S^{2-} species to trigger the full transformation of regular S^{2-} anions into $(S_2)^{2-}$ dimers as observed in pyrite or marcasite.

To some extent, *C*2/*m*-2D FeS_2 exhibits an intermediate charge balance between 2D ($M^{4+}(S^{2-})_2$) and 3D ($M^{2+}(S_2^{2-})$) transition element dichalcogenides. Nevertheless, let us notice that an unconstrained search among possible 2D layers of FeS_2 led us to unravel another dynamically metastable structure that would crystallize in the *P*-1 space group. This structure is more stable than *C*2/*m*-2D, however it is built upon FeS_5 motifs (*vide infra*).

We applied our constrained EA algorithm to the search of the bulk layered structure based on the assembly of *C*2/*m*-2D monolayers. The resulting lowest crystal structure, denoted *C*2/*m*-3D hereafter, consists of the unchanged aforementioned monolayers, well separated from each other by a van der Waals gap (shortest interlayer S-S separation of 3.58 Å). Its structure is displayed in Figure 2(a). We checked that *C*2/*m*-3D is a local minimum on the PES (all frequencies are positive over the Brillouin zone in the phonon dispersion curve in Figure 2b). Bulk *C*2/*m*-3D FeS_2 is an antiferromagnetic semi-conductor with an HSE06 energy gap of 0.84 eV (see the Supporting Information). One can see clearly on its phonon density of states the S_2 dimer signature, *i.e.* a S-S stretching mode computed at 505 cm^{-1} within the harmonic approximation that is in good agreement with the experimental value of 469 cm^{-1} obtained by IR spectroscopy (4 meV difference between experimental and theoretical values).[24] We evaluated the exfoliation energy of *C*2/*m*-3D FeS_2 at 0.26 J/m^2, and its cleavage strength (σ) at 1.40 GPa (see the Supporting Information), which are lower than that of graphite (0.37 J/m^2 [45] and 2.10 GPa[46]). Considering that graphene has been experimentally exfoliated, it is highly probable that a two-dimensional FeS_2 material should be obtained.

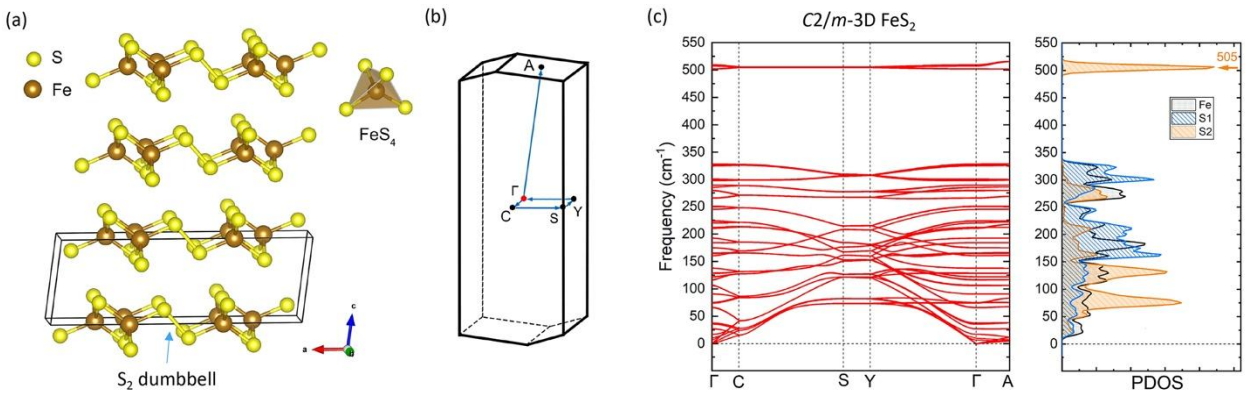

Figure 2. Layered metastable *C*2/*m*-3D FeS_2: (a) Crystal structure and enlightened FeS_4 tetrahedra and S_2^{2-} dumbbells. (b) Brillouin zone for *C*2/*m*-3D, and selected k-path is highlighted; (c) Phonon dispersion curve (left) and phonon DOS (right). S_1 indicates the sulfur belonging to the FeS_4 tetrahedron and S_2 indicates the sulfur atoms belonging to the S_2^{2-} dimer. The arrow indicates a peak at 505 cm^{-1} which is attributed to S-S stretching modes of S_2^{2-} dimers (blue).

To position this structure among the possible 3D FeS_2 compounds, we also performed an unconstrained 3D search along the PES. Only the most relevant and dynamically stable structures are displayed in Figure 3. On the experimental point of view, excluding the specific cases of PdS_2 and $PdSe_2$, IrS_2 and $IrSe_2$, and $RhSe_2$, MQ_2 dichalcogenides (M = transition element, Q = S, Se) are known to display either a layered structural arrangement (*e.g.* TiS_2, MoS_2 and derivatives) or a tridimensional pyrite or marcasite structure.[47] In both cases, metals are six-fold coordinated by anions. Our extensive EA searches on bulk FeS_2 (here only the chemical composition (1 Fe, 2 S) is given with no extra constraints) successfully reproduced the two experimentally known FeS_2 phases, pyrite (*Pa*-3, SG205, *Z*=4) and marcasite (*Pnnm*, SG58, *Z*=2), which are the two most stable structures (see Figure 3 a-b). These two polymorphic structures present a $Fe^{2+}(S_2)^{2-}$ charge balance (higher redox potential of iron in octahedral site than in tetrahedral one)

and mainly differ in how the S_2^{2-} dimers are arranged around the Fe^{2+} cations. The calculated S-S bond lengths are 2.16 Å for pyrite (exp. 2.15 Å)[26] and 2.21 Å (exp. 2.19 Å)[26] for marcasite structures. The relative errors of predicted equilibrium volume of the unit cell with respect to experimental results are as low as 0.5% (159.6 $Å^3$ and 81.9$Å^3$ versus 158.9 $Å^3$ and 81.5 $Å^3$ for pyrite and marcasite, respectively). Both the structural and energetic properties are in very good agreement with the experimental and theoretical data, which validates our methodological approach. Finally, note that the third structure in energy ranking (therefore before the *C*2/*m*-3D that is ranked at the fourth position), to be denoted *P*-1-3D*,* displays 5-coordinated iron atoms and contains both sulfides and persulfides moieties (see Figure 3 c). In this layered material, each S_2 dimer links two [Fe_2S_2] infinite chains as found in *C*2/*m*-3D phase, but here each sulfur atom of a S_2 unit bridges two iron sites within a single chain resulting in 5-coordinated square pyramidal iron atoms. This structural filiation between *C*2/*m* and *P*-1 layers is depicted in the Supporting Information. This new material is predicted to be antiferromagnetic and lies 282 meV/f.u. above the pyrite and 143meV/f.u. below *C*2/*m*-3D. The synthesis of this newly layered five-coordinated *P*-1-3D FeS_2 will be a true challenge.

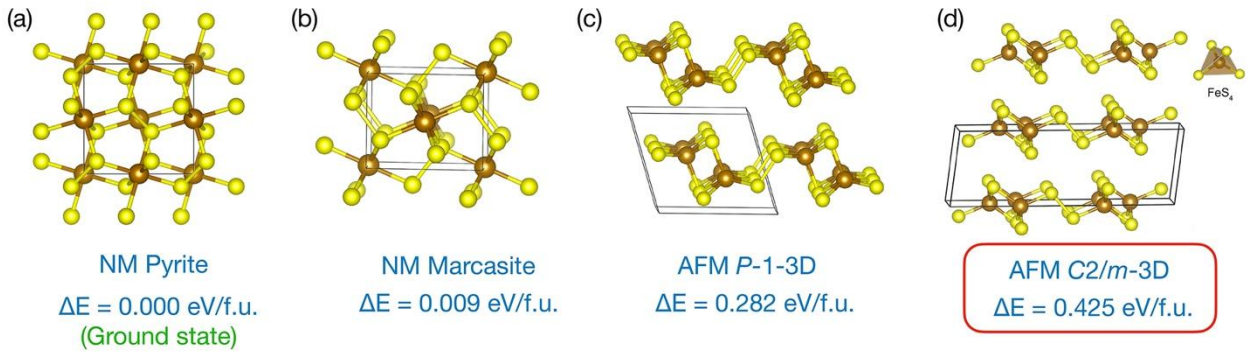

Figure 3. All dynamically stable 3D FeS_2 structures investigated in this paper as a function of their energy. (a) Pyrite. (b) Marcasite. (c) *P*-1-3D. (d) *C*2/*m*-3D. The magnetic properties

(NM=non-magnetic, AFM=antiferromagnetic) are also indicated, with the formation energy relative to the most stable case (3D cubic pyrite, ground state). The properties of the *C*2/*m*-3D structure that meets all experimental criteria is framed in red, and the specific FeS_4 tetrahedral environment of the iron atom is displayed.

To conclude, we performed evolutionary crystal structure prediction searches with prior structural constraints derived from several spectroscopies to investigate the crystal structure of the twice delithiated Li_2FeS_2 compound. We propose a dynamically stable phase *C*2/*m*-2D and its tridimensional derivative *C*2/*m*-3D built upon *C*2/*m*-2D layers as metastable phases with a crystal structure that fully matches the $Fe^{3+}S^{2-}(S_2)^{2-}{}_{1/2}$ formulation issued from Mössbauer, IR and EXAFS spectroscopic measurements. Such an intermediate oxidation level of *C*2/*m*-2D FeS_2 is to be related to its coordination geometry, since Fe in the tetrahedral sites found in *C*2/*m*-2D FeS_2 are stabilized with d^5 high-spin configuration (Fe^{3+}), then being a milder oxidizing agent than Fe in octahedral sites of Fe in pyrite or marcasite that favours d^6 low-spin configuration (Fe^{2+}) to fill its t_{2g} levels. Along our exploration of the energy landscape, we discover the possible existence of another FeS_2 polymorph with five-fold coordinated Fe that would be a challenge to form. Moreover, further work will explore the complexity of the anionic/cationic redox competition in chalcogenides to generate new phases assisted by calculations.

ASSOCIATED CONTENT

Supporting information

Methodological details; calculated structural parameters and energies for all 2D and 3D FeS_2 candidates; magnetic configurations; phonon dispersion curve; DOS-HSE06; COHP; ELF contour plot; *ab initio* molecular dynamics simulations; exfoliation energy; simulated X-Ray diffraction patterns; simulated pair distribution function (PDF) of $Li_{(2-x)}FeS_2$ and polymorphic predicted and experimental FeS_2 phases.

AUTHOR INFORMATION

ORCID

Busheng Wang: 0000-0002-7743-9471

Isabelle Braems: 0000-0003-2374-4259

Shunsuke Sasaki: 0000-0001-8358-1629

Frédéric Guégan: 0000-0002-4932-8643

Laurent Cario: 0000-0001-5720-4395

Stéphane Jobic: 0000-0002-1900-0030

Gilles Frapper: 0000-0001-5177-6691

Notes

The authors declare no competing financial interests.

ACKNOWLEDGMENT

We thank the ANR PRCI Predict_2D_Nanomat (P.I. G.F.), the FEDER and Nouvelle Aquitaine Region (France). We also acknowledge the High-Performance Computing Centers of Poitiers University Mésocentre SPIN, France) and the Irène/TGCC, and Jean Zay/IDRIS GENCI (France) under projects no. X2016087539 and Jean Zay Challenge 2019 for allocation of computing time.

REFERENCES

(1) Zak, A.; Feldman, Y.; Lyakhovitskaya, V.; Leitus, G.; Popovitz-Biro, R.; Wachtel, E.; Cohen, H.; Reich, S.; Tenne, R. Alkali Metal Intercalated Fullerene-like MS_2 (M= W, Mo) Nanoparticles and Their Properties. *J. Am. Chem. Soc.* **2002**, *124* (17), 4747–4758.

(2) Hu, Z.; Wang, L.; Zhang, K.; Wang, J.; Cheng, F.; Tao, Z.; Chen, J. MoS_2 Nanoflowers with Expanded Interlayers as High-Performance Anodes for Sodium-Ion Batteries. *Angew. Chemie Int. Ed.* **2014**, *53* (47), 12794–12798.

(3) Stephenson, T.; Li, Z.; Olsen, B.; Mitlin, D. Lithium Ion Battery Applications of Molybdenum Disulfide (MoS_2) Nanocomposites. *Energy Environ. Sci.* **2014**, *7* (1), 209–231.

(4) Ren, X.; Zhao, Q.; McCulloch, W. D.; Wu, Y. MoS_2 as a Long-Life Host Material for Potassium Ion Intercalation. *Nano Res.* **2017**, *10* (4), 1313–1321.

(5) Zhou, X.; Wilfong, B.; Vivanco, H.; Paglione, J.; Brown, C. M.; Rodriguez, E. E. Metastable Layered Cobalt Chalcogenides from Topochemical Deintercalation. *J. Am. Chem. Soc.* **2016**, *138* (50), 16432–16442.

(6) Wan, J.; Lacey, S. D.; Dai, J.; Bao, W.; Fuhrer, M. S.; Hu, L. Tuning Two-Dimensional Nanomaterials by Intercalation: Materials, Properties and Applications. *Chem. Soc. Rev.* **2016**, *45* (24), 6742–6765.

(7) Murphy, D. W.; Cros, C.; Di Salvo, F. J.; Waszczak, J. V. Preparation and Properties of $LixVS_2$ ($0 < x < 1$). *Inorg. Chem.* **1977**, *16* (12), 3027–3031.

(8) Sinha, S.; Murphy, D. W. Lithium Intercalation in Cubic TiS_2. *Solid State Ionics* **1986**, *20* (1), 81–84.

(9) Rouxel, J.; Danot, M.; Bichon, M. Les Composites Intercalaires Na_xTiS_2. Etude Gènérale Des Phases Na_xTiS_2 et K_xTiS_2. *Bull. Soc. Chim* **1971**, *11*, 3930–3936.

(10) Leblanc-Soreau, A.; Danot, M.; Trichet, L.; Rouxel, J. Les Intercalaires A_xTiS_2 et A_xZrS_2. Structure et Liaisons.(A= Li, Na, K, Rb, Cs). *Mater. Res. Bull.* **1974**, *9* (2), 191–197.

(11) Cousseau, J.; Trichet, L.; Rouxel, J. Behavior of Zirconium Disulfide in Presence of Solutions of Alkali-Metals in Liquid-Ammonia-Intercalates Na_xZrS_2 and K_xZrS_2 and K_xZrS_2 and Phase $(NH_3)ZrS_2$. *Bull. Soc. Chim. Fr.* **1973**, No. 3, 872–878.

(12) Arnaud, Y.; Chevreton, M.; Ahouandjinou, A.; Danot, M.; Rouxel, J. Etude Structurale Des Composés M_xTiSe_2 (M= Fe, Co, Ni). *J. Solid State Chem.* **1976**, *18* (1), 9–15.

(13) Tarascon, J. M.; Vaughan, G.; Chabre, Y.; Seguin, L.; Anne, M.; Strobel, P.; Amatucci, G. In Situ Structural and Electrochemical Study of $Ni_{1-x}Co_xO_2$ Metastable Oxides Prepared by Soft Chemistry. *J. Solid State Chem.* **1999**, *147* (1), 410–420.

(14) Sathiya, M.; Rousse, G.; Ramesha, K.; Laisa, C. P.; Vezin, H.; Sougrati, M. T.; Doublet, M.-L.; Foix, D.; Gonbeau, D.; Walker, W.; others. Reversible Anionic Redox Chemistry in High-Capacity Layered-Oxide Electrodes. *Nat. Mater.* **2013**, *12* (9), 827–835.

(15) Assat, G.; Delacourt, C.; Dalla Corte, D. A.; Tarascon, J.-M. Practical Assessment of Anionic Redox in Li-Rich Layered Oxide Cathodes: A Mixed Blessing for High Energy Li-Ion Batteries. *J. Electrochem. Soc.* **2016**, *163* (14), A2965.

(16) McCalla, E.; Abakumov, A. M.; Saubanère, M.; Foix, D.; Berg, E. J.; Rousse, G.; Doublet, M.-L.; Gonbeau, D.; Novák, P.; Van Tendeloo, G.; others. Visualization of OO Peroxo-like Dimers in High-Capacity Layered Oxides for Li-Ion Batteries. *Science.* **2015**, *350* (6267), 1516–1521.

(17) Subban, C. V; Rousse, G.; Vannier, R.-N.; Laberty-Robert, C.; Barboux, P.; Tarascon, J.-M. Search for Li-Electrochemical Activity and Li-Ion Conductivity among Lithium Bismuth Oxides. *Solid State Ionics* **2015**, *283*, 68–74.

(18) Saha, S.; Assat, G.; Sougrati, M. T.; Foix, D.; Li, H.; Vergnet, J.; Turi, S.; Ha, Y.; Yang, W.; Cabana, J.; others. Exploring the Bottlenecks of Anionic Redox in Li-Rich Layered Sulfides. *Nat. Energy* **2019**, *4* (11), 977–987.

(19) Yahia, M. Ben; Vergnet, J.; Saubanère, M.; Doublet, M.-L. Unified Picture of Anionic Redox in Li/Na-Ion Batteries. *Nat. Mater.* **2019**, *18* (5), 496–502.

(20) Batchelor, R. J.; Einstein, F. W. B.; Jones, C. H. W.; Fong, R.; Dahn, J. R. Crystal Structure of Li_2FeS_2. *Phys. Rev. B* **1988**, *37* (7), 3699.

(21) Hansen, C. J.; Zak, J. J.; Martinolich, A. J.; Ko, J. S.; Bashian, N. H.; Kaboudvand, F.; der Ven, A.; Melot, B. C.; Nelson Weker, J.; See, K. A. Multielectron, Cation and Anion Redox in Lithium-Rich Iron Sulfide Cathodes. *J. Am. Chem. Soc.* **2020**, *142* (14), 6737–6749.

(22) Brec, R.; Prouzet, E.; Ouvrard, G. Redox Processes in the Li_xFeS_2/Li Electrochemical System Studied through Crystal, Mössbauer, and EXAFS Analyses. *J. Power Sources* **1989**, *26* (3–4), 325–332.

(23) Blandeau, L.; Ouvrard, G.; Calage, Y.; Brec, R.; Rouxel, J. Transition-Metal Dichalcogenides from Disintercalation Processes. Crystal Structure Determination and Mossbauer Study of Li_2FeS_2 and Its Disintercalates Li_xFeS_2 ($0.2 \leqslant X \leqslant 2$). *J. Phys. C Solid State Phys.* **1987**, *20* (27), 4271.

(24) Gard, P.; Sourisseau, C.; Ouvrard, G.; Brec, R. Infrared Study of Lithium Intercalated Phases in the Li_xFeS_2 System ($0 \leqslant X \leqslant 2$). Characterization of a New Iron Disulfide. *Solid State Ionics* **1986**, *20* (3), 231–238.

(25) Broderick, J. B. Iron-Sulfur Clusters in Enzyme Catalysis. **2003**.

(26) Schmøkel, M. S.; Bjerg, L.; Cenedese, S.; Jørgensen, M. R. V; Chen, Y.-S.; Overgaard, J.; Iversen, B. B. Atomic Properties and Chemical Bonding in the Pyrite and Marcasite Polymorphs of FeS_2: A Combined Experimental and Theoretical Electron Density Study. *Chem. Sci.* **2014**, *5* (4), 1408–1421.

(27) Grønvold, F.; Westrum Jr, E. F. Heat Capacities of Iron Disulfides Thermodynamics of Marcasite from 5 to 700 K, Pyrite from 300 to 780 K, and the Transformation of Marcasite to Pyrite. *J. Chem. Thermodyn.* **1976**, *8* (11), 1039–1048.

(28) Sun, R.; Chan, M. K. Y.; Ceder, G. First-Principles Electronic Structure and Relative Stability of Pyrite and Marcasite: Implications for Photovoltaic Performance. *Phys. Rev. B* **2011**, *83* (23), 235311.

(29) Zhang, M.-Y.; Cui, Z.-H.; Jiang, H. Relative Stability of FeS_2 Polymorphs with the Random Phase Approximation Approach. *J. Mater. Chem. A* **2018**, *6* (15), 6606–6616.

(30) Spagnoli, D.; Refson, K.; Wright, K.; Gale, J. D. Density Functional Theory Study of the Relative Stability of the Iron Disulfide Polymorphs Pyrite and Marcasite. *Phys. Rev. B* **2010**, *81* (9), 94106.

(31) Huang, B.; Frapper, G. Pressure-Induced Polymerization of CO_2 in Lithium-Carbon Dioxide Phases. *J. Am. Chem. Soc.* **2017**, *140* (1), 413–422.

(32) Huang, B. Computational Materials Discovery: Prediction of Carbon Dioxide and Nitrogen-Based Compounds under Pressure Using Density Functional Theory and Evolutionary Algorithm. Ph.D. Dissertation (supervisor: Pr. G. Frapper), Université de Poitiers: Poitiers, France, 2017. http://theses.univ-poitiers.fr/notice/view/59262.

(33) Oganov, A. R.; Glass, C. W. Crystal Structure Prediction Using Ab Initio Evolutionary Techniques: Principles and Applications. *J. Chem. Phys.* **2006**, *124* (24), 244704.

(34) Oganov, A. R.; Lyakhov, A. O.; Valle, M. How Evolutionary Crystal Structure Prediction Works and Why. *Acc. Chem. Res.* **2011**, *44* (3), 227–237.

(35) Lyakhov, A. O.; Oganov, A. R.; Stokes, H. T.; Zhu, Q. New Developments in Evolutionary Structure Prediction Algorithm USPEX. *Comput. Phys. Commun.* **2013**, *184* (4), 1172–1182.

(36) Zhou, X.-F.; Dong, X.; Oganov, A. R.; Zhu, Q.; Tian, Y.; Wang, H.-T. Semimetallic Two-Dimensional Boron Allotrope with Massless Dirac Fermions. *Phys. Rev. Lett.* **2014**, *112* (8), 85502.

(37) Kresse, G.; Furthmüller, J. Efficient Iterative Schemes for Ab Initio Total-Energy

Calculations Using a Plane-Wave Basis Set. *Phys. Rev. B* **1996**, *54* (16), 11169–11186.

(38) Sun, J.; Ruzsinszky, A.; Perdew, J. P. Strongly Constrained and Appropriately Normed Semilocal Density Functional. *Phys. Rev. Lett.* **2015**, *115* (3), 36402.

(39) Cococcioni, M.; De Gironcoli, S. Linear Response Approach to the Calculation of the Effective Interaction Parameters in the LDA+ U Method. *Phys. Rev. B* **2005**, *71* (3), 35105.

(40) Sabatini, R.; Gorni, T.; De Gironcoli, S. Nonlocal van Der Waals Density Functional Made Simple and Efficient. *Phys. Rev. B* **2013**, *87* (4), 41108.

(41) Peng, H.; Yang, Z.-H.; Perdew, J. P.; Sun, J. Versatile van Der Waals Density Functional Based on a Meta-Generalized Gradient Approximation. *Phys. Rev. X* **2016**, *6* (4), 41005.

(42) Heyd, J.; Scuseria, G. E.; Ernzerhof, M. Hybrid Functionals Based on a Screened Coulomb Potential. *J. Chem. Phys.* **2003**, *118* (18), 8207–8215.

(43) Ataca, C.; Sahin, H.; Ciraci, S. Stable, Single-Layer MX_2 Transition-Metal Oxides and Dichalcogenides in a Honeycomb-like Structure. *J. Phys. Chem. C* **2012**, *116* (16), 8983–8999.

(44) Chou, S. S.; Sai, N.; Lu, P.; Coker, E. N.; Liu, S.; Artyushkova, K.; Luk, T. S.; Kaehr, B.; Brinker, C. J. Understanding Catalysis in a Multiphasic Two-Dimensional Transition Metal Dichalcogenide. *Nat. Commun.* **2015**, *6* (1), 1–8.

(45) Zacharia, R.; Ulbricht, H.; Hertel, T. Interlayer Cohesive Energy of Graphite from Thermal Desorption of Polyaromatic Hydrocarbons. *Phys. Rev. B* **2004**, *69* (15), 155406.

(46) Zhao, S.; Li, Z.; Yang, J. Obtaining Two-Dimensional Electron Gas in Free Space without Resorting to Electron Doping: An Electride Based Design. *J. Am. Chem. Soc.* **2014**, *136* (38), 13313–13318.

(47) Jobic, S.; Deniard, P.; Brec, R.; Rouxel, J.; Drew, M. G. B. David, W.I.F. Properties of the Transition Metal Dichalcogenides: The Case of IrS2 and IrS22. J. Solid State Chem. 1990, 89 (2), 315-327.